SWIFT-XRT-CALDB-06
Release Date: 2nd November 2005
Prepared by Joe Hill and Lorella Angelini
Date Revised: 29th December 2005
Revision 3.0
Pages Changed: All.
Revision Note: Data for the updated boresight in Figures 5, 6 and 8 have been processed using version 6 of the software. Previous revision of this document showed these data processed with version 5.

SWIFT-XRT-CALDB-06:
Boresight Analysis and Correction for the XRT

This document describes the calibration of the flight and ground software position accuracy for both Photon-Counting and Imaging modes. A new boresight has been determined and has been verified for all cases.

Overview

In January 2005, it was discovered that the Spacecraft velocity aiding was effecting the XRT positions. This manifested itself as stellar aberration effects on the positions. Following the de-activation of the velocity aiding at 21:57 31st January 2005[1], additional calibrations of the XRT Image mode were performed on DOY 32, 33 and 34. Furthermore, analysis of these data led to updates of the flight centroiding parameters, which were verified against more calibration data obtained on DOY 60.

After the Flight Software (FSW) update to Build 8.9 on May 27th 2005, there was an event (possibly a micrometeroid impact), which damaged the CCD. Several columns had to be identified as hot pixels in the FSW. To quantify the effect on the centroiding algorithm onboard, and also to determine if the accuracy was affected, several observations of Cygnus X-3 and Cygnus X-1 were taken in Image mode on June 10th 2005.

During the first 6 months that *Swift* was on-orbit, there have been several reports of position degradation with time, although these have never actually been quantified. Nevertheless, to ensure that the boresight calibration is valid for the entire duration on-orbit to date, additional observations of Cygnus X-2 were obtained on 21st October 2005.

From comparing the XRT positions obtained from observations of calibration sources and GRBs with optical counterparts, it was determined that both the ground and the onboard default boresight needed to be calibrated and updated, see Figure 1.

---

[1] Data obtained prior to 21:57 31 January 2005 are corrected for stellar aberration effects in the SDC data processing.
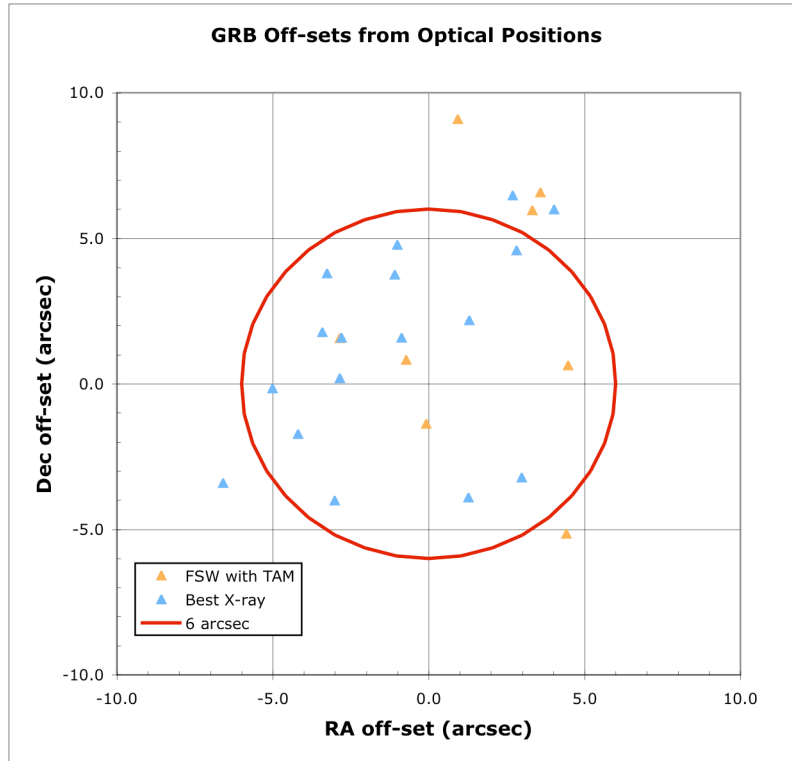
Figure 1. GRB off-sets from Optical positions with a default boresight position of 300x300 comparing the onboard FSW positions with the positions obtained from post-processing the event data on the ground.

Image mode boresight analysis

An *idl* script was written to recalculate the source position for different boresights reproducing the FSW calculation. The script reads in the data from the header of the telemetered postage stamp message obtained in Image mode. It then regenerates the centroid position in RA and DEC with or without the Telescope Alignment Monitor (TAM) correction (Hill et al.). The script positions were verified against the onboard RA and DEC positions for the default boresight position (300 x 300) and found to be identical. The script was run for a matrix of boresight positions for each observation of many calibration sources. A position off-set in RA and DEC was obtained for each observation by comparing the script position with the known optical position. From looking at the average off-set versus boresight position, one can determine the best-fit boresight. For data from the June 10th observations, the 21st October observations and the GRBs, the best-fit boresight was almost constant in the XRT x-axis. The majority of the variation from test-case to test-case was in the XRT y-axis. This analysis was performed for both TAM corrected and non-TAM corrected data.

Ground software boresight analysis

The best-fit boresight position obtained for Image mode was verified against Photon Counting (PC) mode data where the counting statistics are, in general, much improved. 11 sources and 36 observations were selected with a distribution of roll angles (Table 2). To limit the number of variables, this analysis was performed for data which were not corrected by the TAM.

Nine boresight positions were tested in a matrix around the best-fit Image mode boresight (Table 1). The different boresights were accounted for in the ground software teldef calibration file, by changing the offset in the detector coordinates. The data are shown in the Figure 2 for a subset of boresight positions. Additional verification was performed by plotting the off-set in RA and Dec against the roll angle of the observation (see Figure 3), and verifying that there was no accuracy dependence on roll angle.
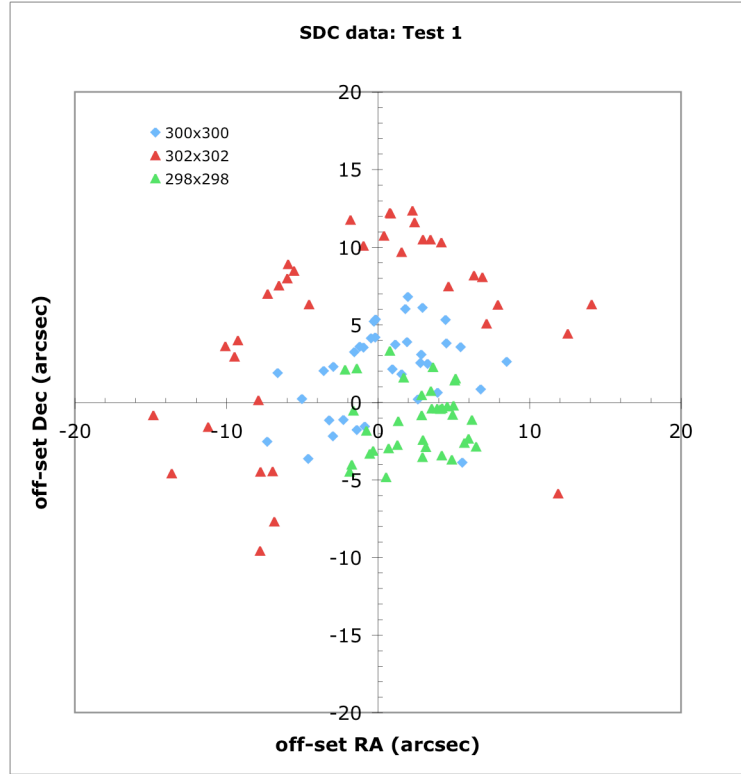

Figure 2. Variation of position off-sets for 36 observations of 11 sources with three boresight positions. Default at 300x300, best estimate from Image mode 298x298 and 302x302 for comparison.
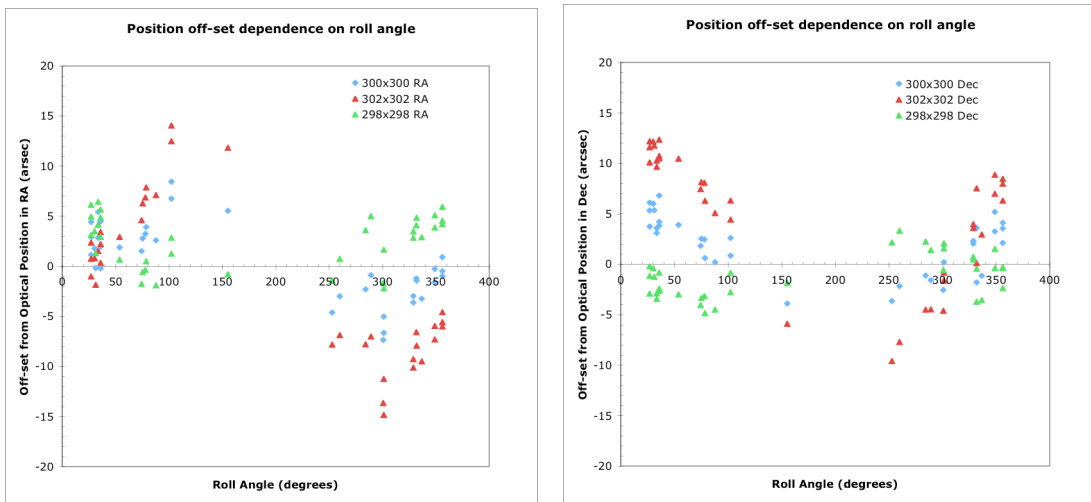

Figure 3. Variation of off-set in RA (left) and Dec (Right) with roll angle for different bore-sight positions; 300x300 (default), 298x298 (best-estimate Image mode) and 302x302 for comparison.

Table 1 The matrix of boresights analysed, showing the mean off-set for the calibration sources.

		X position				
		297	298	299	300	302
	298		3.52		5.72	
Y position	299	3.66	2.62	2.98		
	300		2.58		4.54	
	301		4.18			
	302					10.97
Best Fit	298.2					
	299.3	2.26				

As in the Image mode analysis the average off-sets for each boresight position were plotted against the boresight y- and boresight x-position. From fitting a curve to the data, the boresight was further refined to 298.2 x 299.3 (Figure 4). This was confirmed as the best-fit position by reprocessing the observations with the refined boresight. The mean off-set for the default boresight decreased from 4.5'' to 2.1'' for the new boresight.

SDC best fit boresight

$y = 0.625x^2 - 374.18x + 56007$

$R^2 = 0.9829$

SDC best fit boresight
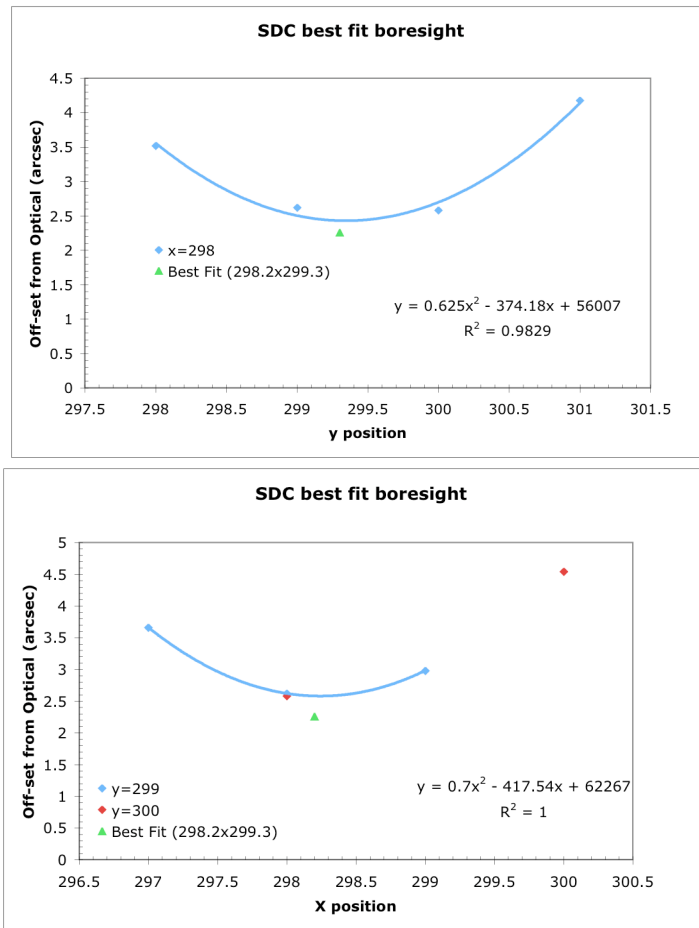
$y = 0.7x^2 - 417.54x + 62267$

$R^2 = 1$

Figure 4. Polynomial fit to the average off-set from the optical position for 36 observations of 11 sources, for 10 boresight positions yeilding a best-fit boresight position of 298.2x299.3.

Following the boresight optimisation, an additional 12 sources were analysed over 35 observations with the new boresight. The average off-set from the optical positions was found to be 2.21'' as seen in the previous sample, with 97% of the positions less than 5'' from the optical position. These data are shown in Figure 6.
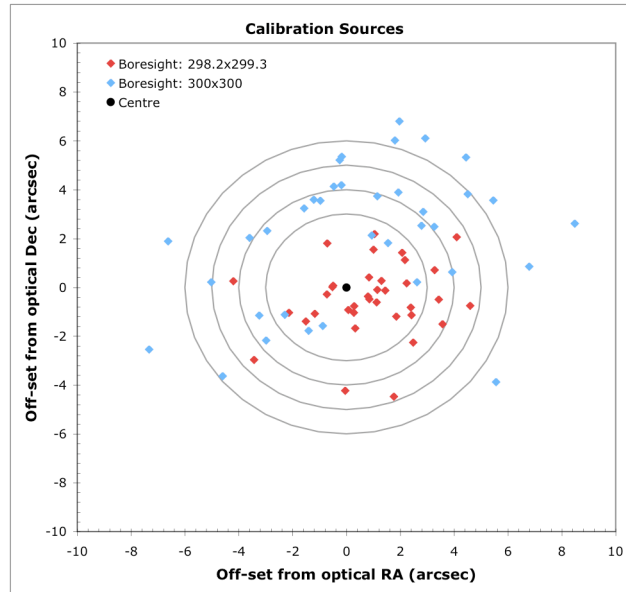
Figure 5. A comparison of calibration source position off-sets from optical positions for the default boresight and for a corrected boresight. The mean off-set for the boresight corrected positions is 2.3'' compared to 4.5'' for the default boresight.

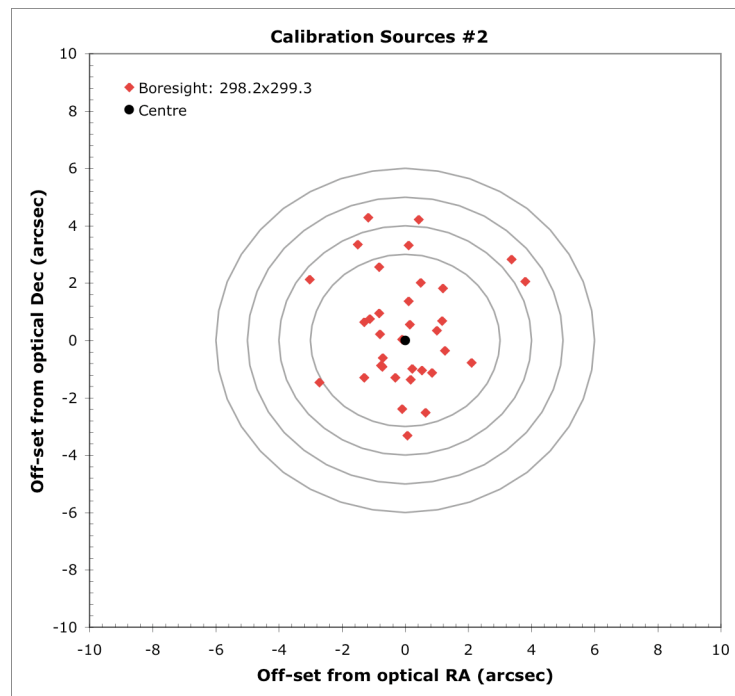**Figure 6. A comparison of additional calibration source position off-sets from optical positions for a corrected boresight. The mean off-set for the boresight corrected positions is 2.2''.**

GRB analysis

A catalogue of 37 GRBs (Table 4) with optical counterparts observed between December 2004 and October 2005 were analysed with the default boresight (Figure 7) and the best-fit boresight position of 298.2 x 299.3 (Figure 8). The average distance from the optical counterpart of 2.3'' was confirmed to be the same as that obtained for the calibration sources.
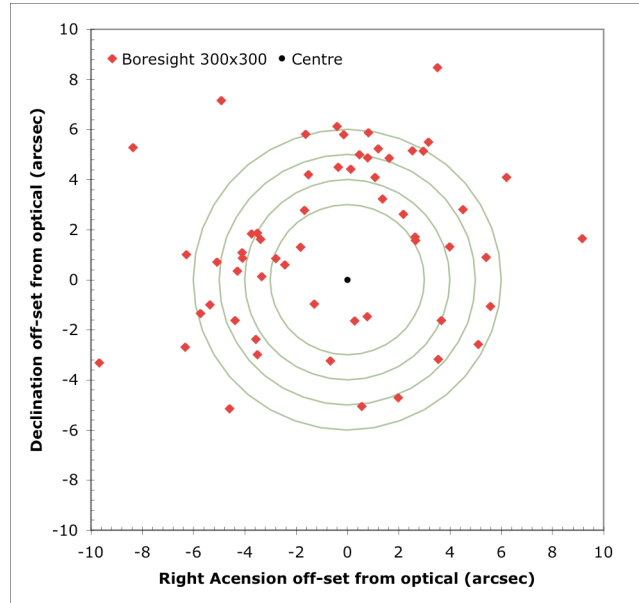
Figure 7. GRB position off-sets from optical positions for the default boresight.
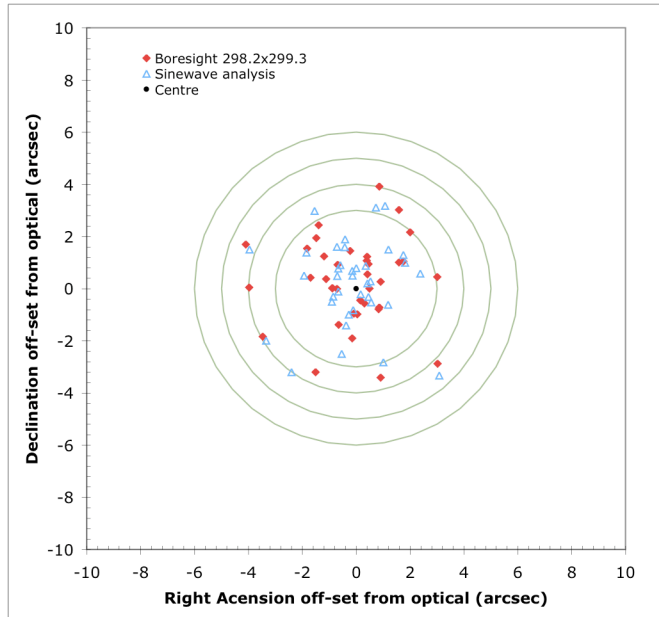
Figure 8. A Comparison of GRB position off-sets from optical positions for a sinewave corrected fit and using a corrected boresight.

A parallel analysis of the GRB positions was performed by plotting the RA and Dec off-sets relative to the optical counterpart against boresight and fitting a sinewave, the details are described in Morreti et al. We find that the implied boresight derived from the sinewave

analysis is consistent with the value obtained in this analysis. A plot of the position off-set of the GRBs from the optical counter-parts obtained by the two methods is shown in Figure 8.

In this analysis the TAM correction has not been applied. Preliminary results presented at the XRT Team Meeting in October (and in Hill et al.) using the default boresight (300 x 300), showed that the position accuracy was improved when the data were TAM corrected however, the positions show a residual off-set compared to those obtained with the new boresight. We find from preliminary analysis of the TAM correction with the new boresight, that the position accuracy is degraded. This is an indication that the TAM correction and the boresight position are not independent variables.

Calibration observations have been made in Image mode with the updated boresight position and confirm an improved FSW position accuracy.

Error analysis

A detailed error analysis has been performed and is documented in SWIFT-CALDB-07.

Teldef updates

This best-fit boresight was implemented as an off-set in the teldef file (version 5) corresponding to a shift in the detector coordinates. In this way, the internal XRT detector coordinate system is no longer maintained. The algorithm used to derive the time of the events for the Timing modes uses the internal XRT detector coordinate system. The shift in the detector coordinates for the boresight correction introduces a small time shift (one row or less) to the Timing mode data. To maintain the XRT internal detector coordinate definition, the shift in the boresight can be included as a small misalignment in the matrix that translates the detector coordinates into sky coordinates. This change has been applied in version 6 of the teldef file. The two different teldefs (version 5 and 6) produce identical results when applied to data files derived with the same screening criteria and software release.

Table 2: Sources and observations selected for testing a matrix of different boresights to derive the best-fit boresight. The table includes source name, sequence number, RA and Dec of the optical source position, start time of the observation, the roll angle and the XRT PC mode exposure.

Source name	Observation ID	Optical position: Right Ascension	Optical position: Declination	Start time (UTC)	Roll angle (degrees)	XRT exposure PC mode (Seconds)
NGC5548	30022004	14 17 59.65	+25 08 13.4	4/8/05 8:40	35.79522	440.41
NGC5548	30022005	14 17 59.65	+25 08 13.4	4/8/05 11:52	35.80822	242.24
NGC5548	30022006	14 17 59.65	+25 08 13.4	4/8/05 15:06	35.79035	277.52
NGC5548	30022014	14 17 59.65	+25 08 13.4	4/10/05 7:18	33.49466	1498.63
NGC5548	30022015	14 17 59.65	+25 08 13.4	4/9/05 18:31	33.49481	1307.12
NGC5548	30022033	14 17 59.65	+25 08 13.4	4/12/05 13:56	30.18841	317.15
NGC5548	30022040	14 17 59.65	+25 08 13.4	4/14/05 15:49	26.90384	287.19
NGC5548	30022045	14 17 59.65	+25 08 13.4	4/14/05 17:25	26.90242	292.18
NGC5548	30022046	14 17 59.65	+25 08 13.4	4/14/05 19:03	26.89817	292.18
NGC5548	30022048	14 17 59.65	+25 08 13.4	4/26/05 9:52	356.10055	220.62
NGC5548	30022047	14 17 59.65	+25 08 13.4	4/26/05 10:56	356.09505	1030.48
NGC5548	30022049	14 17 59.65	+25 08 13.4	4/26/05 12:35	356.08969	1043.02
NGC5548	30022054	14 17 59.65	+25 08 13.4	5/10/05 17:07	348.78813	1055.57
NGC5548	30022055	14 17 59.65	+25 08 13.4	5/10/05 19:00	348.78329	814.86
QSO J2253+1608	30024001	22 53 57.75	+16 08 53.56	5/11/05 14:41	77.86438	1426.63
QSO J2253+1608	30024002	22 53 57.75	+16 08 53.56	5/19/05 12:36	74.28865	4522.92
OJ287	35011001	08 54 48.87	+20 06 30.64	5/20/05 5:14	289.01704	3715.63
OJ287	35011003	08 54 48.87	+20 06 30.64	6/7/05 13:35	284.16883	1253.64
Mkn421	35014002	11 04 27.31	+38 12 31.80	4/1/05 4:08	331.8063	385.31
Mkn180	35015001	11 36 26.41	+70 09 27.3	4/16/05 0:24	328.73897	2943.45
Mkn180	35015002	11 36 26.41	+70 09 27.3	4/18/05 3:23	328.73572	6398.48
Mkn501	35023001	16 53 52.22	+39 45 36.61	4/21/05 1:01	53.75609	546.56
Mkn501	35023002	16 53 52.22	+39 45 36.61	6/17/05 22:41	351.66501	1835.32
BLLac	35028001	22 02 43.29	+42 16 39.98	7/25/05 22:08	31.27963	566.51
3C454.3	35030001	22 53 57.75	+16 08 53.56	4/24/05 18:38	87.84266	13724.1
3C454.3	35030003	22 53 57.75	+16 08 53.56	5/17/05 16:18	75.2958	4771.34
AKN564	35062001	22 42 39.47	+29 43 30.0	4/19/05 15:28	102.32689	4605.84
AKN564	35062256	22 42 39.47	+29 43 30.0	4/27/05 0:39	102.29757	4675.91
AKN564	35062002	22 42 39.47	+29 43 30.0	5/19/05 0:22	78.56376	4410.25
Mkn684	35078001	14 31 04.7	+28 17 13	7/14/05 9:48	301.20647	4758.83
Mkn684	35078002	14 31 04.7	+28 17 13	7/14/05 9:28	301.19094	386.09
Mkn684	35078004	14 31 04.7	+28 17 13	7/15/05 5:06	300.5782	589.18
Mkn684	35078006	14 31 04.7	+28 17 13	9/15/05 0:39	259.77146	12907.5
Mkn684	35078007	14 31 04.7	+28 17 13	9/18/05 2:52	252.72212	8226.22
Mkn421	52100009	11 04 27.31	+38 12 31.80	10/4/05 4:19	155.17124	8048.35
Mkn813	56600002	14 27 25.06	+19 49 51.5	5/20/05 10:57	336.63431	707.03

Table 3: Sources and observations selected as control sample for the best-fit boresight position. The table includes source name, sequence number, RA and Dec of the optical source position, start time of the observation and the XRT PC mode exposure.

Source name	Observation ID	Optical position: Right Ascension	Optical position: Declination	Start time (UTC)	Roll angle (degrees)	XRT exposure PC mode (Seconds)
PKS0537-441	30138001	05 38 50.36	-44 05 08.939	7/12/05 0:02	27.14861	4978.46
1ES0120+340	35000001	01 23 08.90	+34 20 50	6/9/05 16:57	78.77028	1607.15
PKS0208-512	35002001	02 10 46.20	-51 01 01.89	4/22/05 23:43	359.884	12300.7
PKS0208-512	35002003	02 10 46.20	-51 01 01.89	5/5/05	10.71307	2030.87
PKS0208-512	35002004	02 10 46.20	-51 01 01.89	5/12/05 0:19	17.25286	2108.62
PKS0208-512	35002005	02 10 46.20	-51 01 01.89	5/10/05 0:15	15.41735	4114.37
3C66A	35003001	02 22 39.61	+43 02 07.80	6/29/05 10:56	89.80221	5025.83
1H0323+022	35006001	03 26 13.97	+02 25 14.70	6/26/05 13:15	59.91305	10741.1
1H0323+022	35006002	03 26 13.97	+02 25 14.7	6/29/05 17:26	61.34463	4676.07
1H0323+022	35006003	03 26 13.97	+02 25 14.7	7/11/05 2:51	65.42399	6586.64
1ES1011+496	35012002	10 15 04.17	+49 26 00.6	6/19/05 19:17	267.536	7998.24
1ES1011+496	35012003	10 15 04.17	+49 26 00.6	6/26/05 7:14	262.2681	9157.33
1H1100-230	35013001	11 03 37.57	-23 29 30.2	6/30/05 0:06	300.8013	8554.73
1ES2344+514	35031002	23 47 04.92	+51 42 17.9	5/19/05 16:09	101.353	4199.69
1H1426+428	35020003	14 28 32.50	+42 40 25	4/2/05 17:59	32.42575	1293.879
H1426+428	51000002	14 28 32.50	+42 40 25	6/19/05 4:56	319.449	21462.5
H1426+428	51000003	14 28 32.50	+42 40 25	6/25/05 5:54	314.8236	22908.6
1ES2344+514	35031001	23 47 04.92	+51 42 17.9	4/19/05 0:30	136.6156	4683.53
1ES2344+514	35031002	23 47 04.92	+51 42 17.9	5/19/05 16:09	101.3537	4199.69
PKS0823-223	35071001	08 26 01.57	-22 30 27.20	6/20/05 23:51	320.5244	2908.4
PKS0823-223	35071002	08 26 01.57	-22 30 27.20	7/1/05 0:10	329.8242	20367.9
PKS0823-223	35071003	08 26 01.57	-22 30 27.20	7/3/05 0:19	332.4729	31355.1
PKS0823-223	35071004	08 26 01.57	-22 30 27.20	9/6/05 3:41	57.23821	7376.38
PKS0823-223	35071005	08 26 01.57	-22 30 27.20	9/22/05 20:39	82.62095	5106.88
PKS0823-223	35071006	08 26 01.57	-22 30 27.20	9/28/05 9:11	85.8729	5887.07
PKS0823-223	35071007	08 26 01.57	-22 30 27.20	9/28/05 18:45	87.0129	8938.38
PKS0823-223	35071008	08 26 01.57	-22 30 27.20	9/29/05 18:27	86.41886	16161.8
PKS0823-223	35071009	08 26 01.57	-22 30 27.20	10/2/05 7:05	90.11244	12395.4
RXJ0148.3-2758	35075002	01 48 22.33	-27 58 25.7	5/5/05 23:59	22.16315	7742.409
RXJ0148.3-2758	35075003	01 48 22.33	-27 58 25.7	5/7/05 0:00	24.21947	22128.31
RXJ0148.3-2758	35075004	01 48 22.33	-27 58 25.7	5/11/05 0:26	27.13348	8875.74
RXJ0148.3-2758	35075006	01 48 22.33	-27 58 25.7	5/13/05 0:18	29.059	3144.09
Mkn728	35168001	11 01 01.77	+11 02 48.3	7/14/05 1:32	290.9755	4488.03
Mkn728	35168003	11 01 01.77	+11 02 48.3	10/24/05 20:51	105.8357	6561.35
Mkn915	35169001	22 36 46.50	-12 32 42.6	7/10/05 23:31	78.29587	2938.509

Table 4: GRBs with confirmed optical counterparts used for the boresight analysis.

GRB Name	Observation ID	RA of optical counterpart	Dec of optical counterpart
GRB 041223	100585001	100.1971	-37.0729
GRB 050126	103780000	278.1132	42.3704
GRB 050219b	106442000	81.3166	-57.7580
GRB 050315	111063000	306.4754	-42.6006
GRB 050318	111529000	49.7125	-46.3956
GRB 050319	111622000	154.1996	43.5485
GRB 050401	113120000	247.8700	2.1873
GRB 050406	113872000	34.4679	-50.1875
GRB 050408	20004001	180.5722	10.8528
GRB 050412	114485000	181.1044	-1.2010
GRB 050416a	114753000	188.4775	21.0574
GRB 050502b	116116000	142.5418	16.9967
GRB 050505	117504000	141.7638	30.2733
GRB 050509a	118707000	310.5817	54.0716
GRB 050525	130088000	278.1358	26.3399
GRB 050603	131560001	39.9868	-25.1819
GRB 050607	132247000	300.1783	9.1421
GRB 050712	145581000	77.7004	64.9132
GRB 050713a	145675000	320.5400	77.0747
GRB 050714b	145994000	169.6988	-15.5477
GRB 050716	146227000	338.5864	38.6843
GRB 050721	146970000	253.4355	-28.3811
GRB 050724	147478000	246.1849	-27.5410
GRB 050726	147788000	200.0496	-32.0644
GRB 050730	148225000	212.0714	-3.7716
GRB 050801	148522000	204.1475	-21.9283
GRB 050802	148646000	219.2737	27.7867
GRB 050814	150314000	264.1891	46.3393
GRB 050815	150532000	293.5965	9.1465
GRB 050820a	151207000	337.4088	19.5603
GRB 050824	151905001	12.2338	22.6089
GRB 050826	152113000	87.7566	-2.6432
GRB 050904	153514000	13.7117	14.0861
GRB 050908	154112000	20.4613	-12.9544
GRB 050915a	155242000	81.6868	-28.0165
GRB 050922c	156467000	317.3879	-8.7583
GRB051016b	159994000	132.1159	13.6556

References

Hill, J.E. et al., "The unique operating modes of the Swift X-ray Telescope", 2005, Proc. SPIE, 5898, 589815-1

Moretti et al, Astronomy & Astrophysics, 2005, submitted